

Article

Not peer-reviewed version

---

# Low-Cost UAV Photogrammetry and GNSS Technology for Digital Terrain Modeling: The DIACHRONIC LANDSCAPES Workshop Case

---

[Andrea Sterpin](#) and [Marco Medici](#) \*

Posted Date: 20 June 2023

doi: 10.20944/preprints202306.1355.v1

Keywords: Workshop; Landscape surveying; Unmanned aerial vehicle (UAV); GNSS; Photogrammetry; Digital terrain model (DTM); Digital elevation model (DEM); Accuracy assessment; Ground control points; Quality check points (QCP).



Preprints.org is a free multidiscipline platform providing preprint service that is dedicated to making early versions of research outputs permanently available and citable. Preprints posted at Preprints.org appear in Web of Science, Crossref, Google Scholar, Scilit, Europe PMC.

Copyright: This is an open access article distributed under the Creative Commons Attribution License which permits unrestricted use, distribution, and reproduction in any medium, provided the original work is properly cited.

## Article

# Low-Cost UAV Photogrammetry and GNSS Technology for Digital Terrain Modeling: The DIACHRONIC LANDSCAPES Workshop Case

Andrea Sterpin and Marco Medici \*

Department of Architecture, University of Ferrara, via Ghiara 36, 44121 Ferrara, Italy; andrea.sterpin@unife.it

\* Correspondence: marco.medici@unife.it; Tel.: +39-0532-293677

**Abstract:** This study examines the activities conducted at the archaeological site of Aptera in Crete, Greece. The research was part of the DIACHRONIC LANDSCAPES International Design Workshop, organized by the CAM (Center for Mediterranean Architecture), TUC (Technological University of Crete School of Architecture), and UNIFE (University of Ferrara Department of Architecture). This article outlines the methods used for data acquisition and processing on a territorial scale, which generated digital outputs necessary for the analysis and design phases of the workshop, as well as for further examination of the results. The collected data, obtained through low-cost aerial photogrammetric surveying and GNSS terrestrial coordinate detection, were integrated in a Structure from Motion workflow that led to the creation and exportation of various digital outputs, such as point clouds, DTM, DSM, orthophotos, and contour lines. An accuracy analysis was performed to evaluate the effectiveness and efficiency of the digital models compared to the implemented surveying strategies, including the Ground Control Point and Quality Check Point marker positioning strategy. The resulting digital models proved to be valuable assets for analysis and design within the workshop and provided insightful prospects for future research and territorial-scale projects.

**Keywords:** workshop; landscape surveying; Unmanned aerial vehicle (UAV); GNSS; photogrammetry; digital terrain model (DTM); digital elevation model (DEM); Accuracy assessment; ground control points; Quality check points (QCP).

## 1. Introduction

In land surveying, technology has significantly evolved in recent years, leading to significant progress in surveying instrumentation and methodologies. Today, it is common to use tools such as total stations, GNSS, terrestrial laser scanning, LiDAR, and UAVs equipped with digital cameras for surveying soils, landscapes, and buildings. Each instrument has specific performance and distinct advantages, depending on the needs of the surveying project [1,2].

This paper will delve into photogrammetric techniques and methodologies derived from UAVs due to their numerous advantages in terms of cost, inspection, surveillance, reconnaissance, and mapping [3].

Recently, digital photogrammetry softwares have advanced significantly, enabling engineers and scientists to create high-resolution topographic maps with low-cost optical cameras for UAS data collection and analysis [4]. As reported in Jimenèz-Jimenèz et al. (2021), *UAV photogrammetry's main advantage is its capacity for direct, rapid, and detailed image capture of a study area with minimum fieldwork. These characteristics lead to cost reductions and much faster project completion, in addition to the possibility to remotely survey complex, inaccessible, and hazardous objects and areas* [2] (p. 2). Moreover, nowadays the Structure-from-Motion (SfM) softwares used in the field of digital photogrammetry can produce 3D topographic outputs – such as *orthorectified imagery maps (orthophotos), point clouds, digital elevation models (DEMs), textured 3D models, contour lines, etc - in a reasonably automated way, with a spatial resolution in the order of centimeters – a quality vital to topographic mapping applications* [1] (p. 2).

One of the main objectives of land surveying is the generation of Digital Elevation Models (DEMs) and derivatives.

DEM (digital elevation model): General term for a digital representation of elevations (or height) of a topographic surface [5] (p. 7).

The term “model” within DEM has multiple meanings, and different communities interpret it differently [5] (p. 2). DEMs can be represented by Image method or Mathematical method. Various data structures have been tried for storing and displaying topographic surfaces [6] (p. 1), for example:

- Rectangular Grid – Image method: Grids are matrix structure that implicitly records topological relation between data points. The data structure of Grid is similar to the array storage structure of digital computers. Raster type DEM is included in it. Raster is a grid of digital, uniform, square cells covering an area on the earth’s surface where each cell is given a value of whatever you want to map. In the case of DEMs, each cell is given the elevation value of the land (or water) surface that it overlies [6] (p. 2).
- Triangulated Irregular Network (TIN) – Mathematical method: The TIN model was developed as a simple way to build a surface from a set of irregularly spaced points. They are vector type data. It utilizes digital points, lines and polygons to represent features on the earth’s surface [6] (p. 2), and the density of the triangles can vary with terrain complexity and slope [5] (p. 6).
- Contours – Mathematical method: A vector representation of topography with isolines of constant elevation. The contour interval can change with terrain complexity and slope [5] (p. 6).

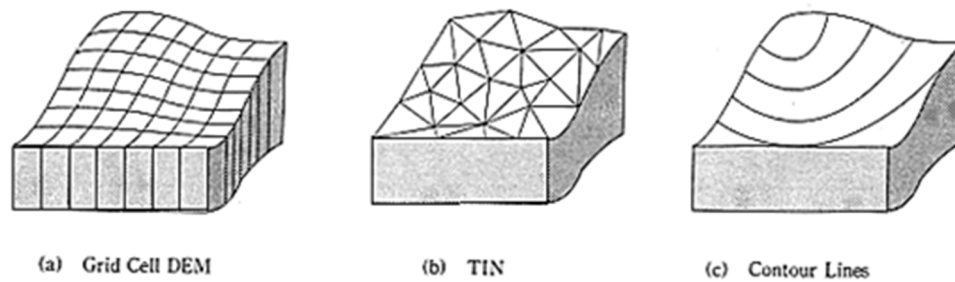


Figure 1. Types of Digital Elevation Models (DEM) [7] (p. 47).

In today’s scenario Grid & TIN are most widely used data structures to create DEMs. In the workflow described in this paper, both will be used. Specifically, the term “DEM” will be used to identify the Grid data structure (in continuity with Guth et al. (2021) [5]), and “DEM (TIN)” to identify the surface mesh-based data structure.

Having defined what is meant by the term “DEM”, it is now necessary to distinguish between DEM, DSM, and DTM.

- DTM (digital terrain model): A DEM that records the boundary between the lithosphere and the atmosphere, without biosphere and anthroposphere, also called a “bare-earth” DEM. The treatment of hydrosphere, cryosphere, and voids (e.g., excluded buildings, water and trees) must be specified and clearly localized, e.g., by respective masks [3] (p. 7) (Figure 2).
- DSM (digital surface model): A DEM that records the lower boundary of the atmosphere [5] (p. 7) (and either the lithosphere, hydrosphere, cryosphere, biosphere or anthroposphere) (Figure 2).

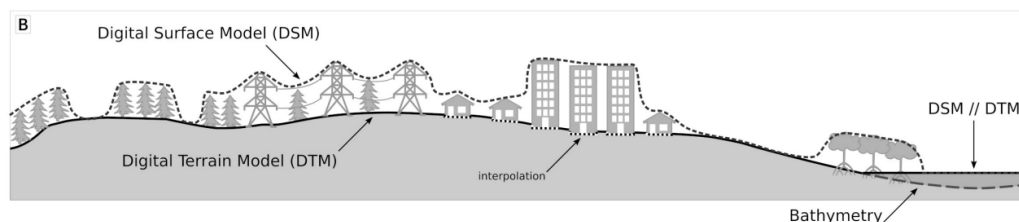


Figure 2. DTM and DSM definition [3].

In the process of generating DTMs, non-terrain objects such as higher vegetation-horizons and buildings are removed through filtering, which is the process of obtaining bare earth. This filtering step is crucial to differentiate points from the ground surface and non-ground features for almost all topographic applications. However, distinguishing between ground and non-ground points can be challenging, especially in regions with high surface variability [8].

Digital Terrain Models (DTMs) and Digital Surface Models (DSMs) are fundamental tools in various fields of application, including:

1. Civil engineering: both DTMs and DSMs are used for the design of infrastructure such as roads, bridges, and dams. They allow for detailed and precise altitude analysis, facilitating the planning and implementation of such works.[9]
2. Urban planning: through the use of DSMs, it is possible to analyze the territory and settlements in detail, evaluate hydraulic risks, provide useful information for sustainable urban development, and disaster prevention. [10,11]
3. Land and environmental management: both DTMs and DSMs are key tools for land, landscape, and vegetation planning, as well as for the evaluation of geological and hydraulic risks. They can also be used for historical-geological reconstructions, contributing to the understanding and conservation of natural heritage. [11–13]
4. Cartography: DTMs are essential for creating maps and digital models of the terrain. Thanks to their precision, these models allow for accurate representations of the earth's relief, helping to determine and analyze morphometric data and parameters. [14,15]
5. Archaeology: Both DSMs and DTMs are valuable tools for detecting archaeological sites. They allow for the identification of anomalies in the landscape that may indicate the presence of ancient structures or settlements, facilitating field investigations. [16]

For the purpose of this paper, the fields of interest mainly concern archaeology and land-environmental management, for which both DTM and DSM models have been produced.

When assessing the quality of a Digital Elevation Model (DEM), *is crucial to evaluate precision, accuracy and comparison with the actual topography terrain* [17] (p. 3). As reported in Ariza López et al. (2008), *the positional accuracy of cartographic products (...) is the quality element of geographic information most extensively used by the national mapping agencies (NMAs), and also the more commonly evaluated quality element option* [18] (p. 1). As reported in Jimenéz-Jiménez et al. (2021), *the positional accuracy requirements for a DEM are directly related to its intended use. (...) Several authors have studied the parameter DEMs accuracy obtained with UAV photogrammetry* [2] (p. 2).

DEMs obtained from micro-UAV images using SfM photogrammetry are influenced by factors like flight design, camera quality and calibration, SfM algorithms, and georeferencing strategies. Determining the appropriate number of ground control points (GCPs) is important to enhance its precision and quality. [19]

Chapter 2, "Materials and Methods," will include a brief presentation of the workshop objectives, an introduction of the adopted instrumentation, and an outline of the techniques and workflows employed for georeferenced photogrammetric surveying. Furthermore, the subsequent data processing will be discussed, specifically through the use of Agisoft Metashape software.

In Chapter 3, "Results," the outputs produced during the workshop will be presented, including the generated DEMs and their specific utilization for the workshop purposes. The quality and accuracy of these DEMs will be thoroughly analyzed and assessed.

Finally, in Chapter 4, "Discussion," final considerations will be developed based on the results obtained, in relation to the extent of the area, the tools used, the adopted methodologies, and the time available and employed.



## 2. Materials and Methods

### 2.1. *The DIACHRONIC LANDSCAPES workshop:*

The work presented in this paper stems from the experience of the DIACHRONIC LANDSCAPES 2023 international design workshop, held at CAM in La Chania (Crete, Greece) from April 3-7 2023 and organized by:

- CAM - Center for Mediterranean Architecture (Prof. Dimitris Tsakalakis)
- TUC - Technological University of Crete School of Architecture (Prof. Panita Karanamea)
- DA UNIFE - University of Ferrara Department of Architecture (Prof. Gianni Lobosco and Prof. Elena Dorato)

Diachronic Landscapes is a multidisciplinary workshop that brings together students and scholars in landscape architecture, urban and territorial planning, and archaeology to explore issues related to landscape heritage understanding, preservation, and promotion.

This collaborative endeavor was based on the collection, interpretation, and design processing of existing data on the archaeological site of Aptera, Crete, combined with new surveys and analyses that informed a strategic landscape plan for the area and its surrounding context. The workshop aimed to produce design ideas and an integrated management plan that could coordinate and combine scheduling and prioritization of archaeological excavations with landscape and territorial design interventions that would enhance the touristic, educational, and overall cultural experience of the site with the support of the Ephorate of Antiquities.

Prior to - and almost concurrently with - the design phase of the workshop, it was necessary to carry out surveys, process the collected data, and provide operational materials in a very short time for the development of the students' projects and documentation materials for the site's curatorial authority.

The operational materials referred to are as follows:

- Dense point cloud with element classification;
- DEMs: DTM and DSM;
- DEMs-TIN: DSM mesh model and DTM mesh model, with texture;
- Orthophotos;
- Contour lines.

The objective of this paper is to describe the surveying, data processing, and output generation workflow for the purposes of the workshop, analyzing step by step the tools and software used, the time taken, and, above all, the quality and accuracy of the results obtained.

### 2.2. *The case study: the plateau of Aptera*

Aptera is an ancient city situated in Greece, near Souda Bay, Crete. It is located on a plateau that spans approximately 250 hectares.

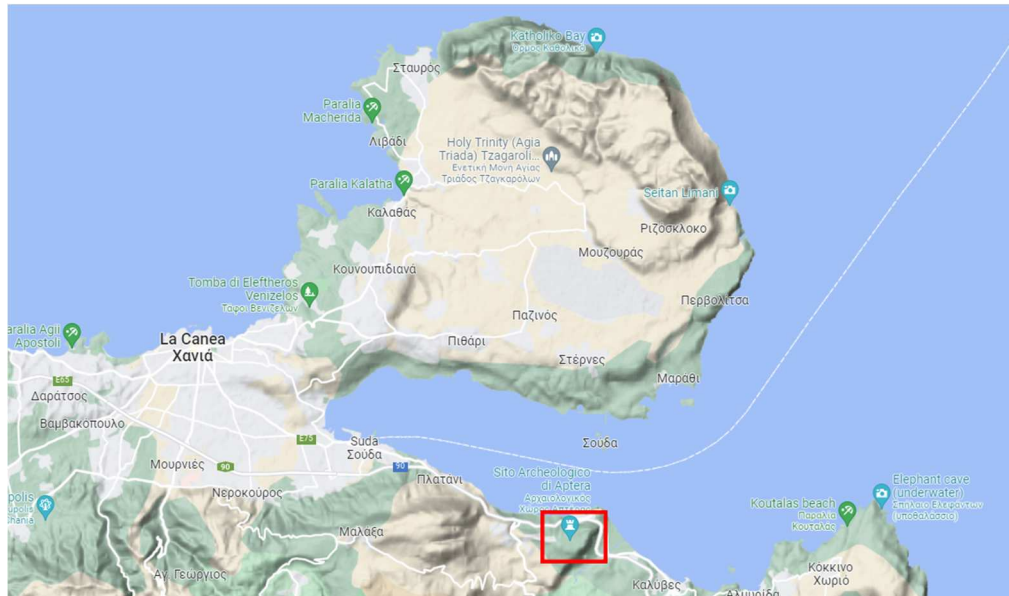


**Figure 3.** Google maps – the Souda bay.



**Figure 4.** Google maps – the Aptera plateau.

Now managed by the Greek Ministry of Culture, Ephorate of Antiquities, over the centuries, the site has experienced various occupations and influences:

1. Minoan civilization (2600 BC - 1100 BC): the oldest occupation of Aptera. Remains of houses, tombs, and everyday objects have been found.
2. Second Minoan civilization (2600 BC - 1100 BC): the oldest occupation of Aptera. Remains of houses, tombs, and everyday objects have been found.
3. Classical period (480 BC - 323 BC): Aptera became an independent Greek city-state and the theater was built. Roman period (323 BC - 395 AD): during this period, the baths, the thermal baths, and the Roman forum were built.
4. Byzantine period (395 AD - 1204 AD): new walls and fortifications were built to protect the city from Arab invasion, and it is believed that an earthquake in the 7th century caused the disappearance of the ancient city.
5. Venetian period (1204 AD - 1669 AD): during this period, Aptera was occupied by the Venetians, who built a castle and fortifications.
6. Ottoman period (1669 AD - 1898 AD): during the Ottoman occupation, the castle was used as a prison and a defensive place.

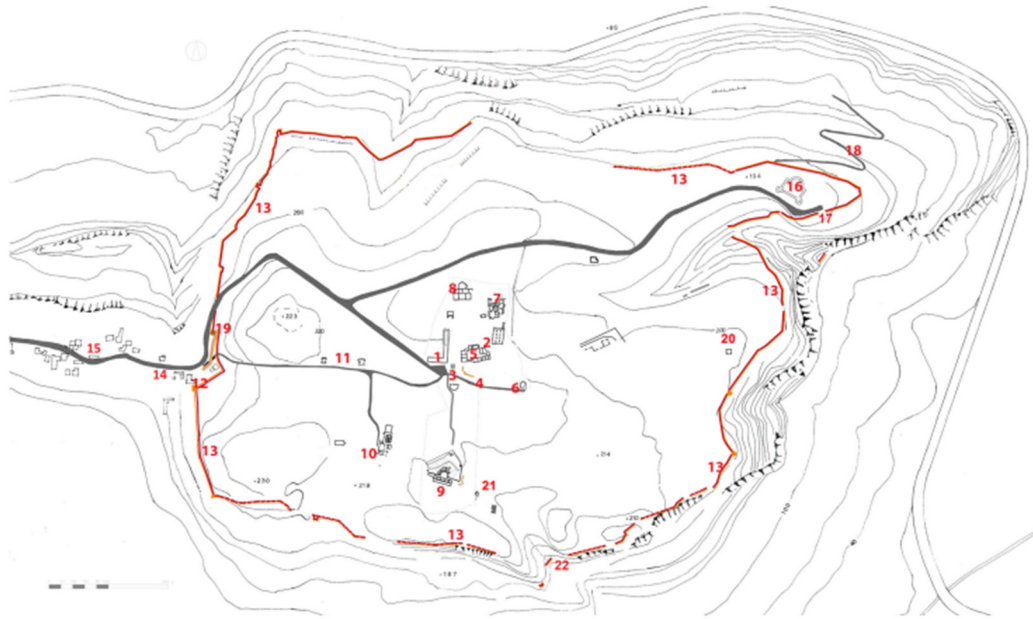


**Figure 5.** Topographical plan of Aptera [20] (p. 17)

### 2.3. Aerial photogrammetric survey

The surface area to be mapped is approximately 250 hectares. To ensure a comprehensive and accurate survey of the area, it was decided to proceed via aerial photogrammetry using a low-cost drone, with automated flight through planning and support - during the photogrammetric reconstruction phase - of GPS coordinates acquired through a GNSS antenna.

#### 2.3.1. Unmanned aerial system (UAS)

For the aerial photogrammetry work via UAV, the DJI Mini 2 drone was used. Our Unmanned Aircraft System (UAS) included two DJI Mini 2 drones, two DJI-RC-N1 controllers, 9 batteries, and two power banks for the continuous recharging of depleted batteries. As we will see in the flight planning phase, equipping ourselves with multiple drones, controllers, and batteries proved necessary to face the vast extents of the area and the windy conditions (from 8 to 30 km/h) prevailing in the project area. Wind indeed represents a critical factor that impacts the battery life and the efficiency of the survey mission. It is also crucial to pay close attention to ensure that the wind or any gusts do not exceed the dynamic capabilities of the drone itself which, in the case of the Mini 2, guarantees a maximum wind resistance of up to 36 km/h.

#### 2.3.2. Initial flight strategy

Given the extensive nature of the case study and the necessity to adhere to tight survey timelines for the workshop, an automated survey flight through planning was chosen rather than manual. Flight planning allowed for the optimization of survey times, the reduction of operator errors, and ensured the acquisition of predefined results, thanks to the a priori definition of parameters such as: this:

- the percentage of vertical and horizontal overlap between successive shots,
- flight altitude,
- confinement of the flight area,
- the pattern of the flight path,
- UAV speed,
- flight duration,
- the number of batteries to be used,
- the desired resolution of the orthophotogrammetric output.



However, it's important to emphasize that office flight programming is not sufficient to ensure the mission's success. Indeed, it's necessary to inspect the area before initiating the flight to identify potential obstacles or dangers that could not be detected beforehand, such as poles, pylons or electrical wires, and potentially modify the flight plan accordingly, as described in Chapter 2.3.3.

For this case study, we opted for the Dronelink software solution, which offers a web app for PC flight mission planning and a smartphone app for mission planning, drone connection, and control during flight. Dronelink offers various features depending on the chosen plan, divided between professional plans (periodic payment with three solutions: starter, growth, and enterprise) and hobbyistic plans (one-time payment with three solutions: basic, premium, and elite). For this case study, we adopted the premium plan, which proved ideal for planning areas and micro-areas with nadir flight at a constant height.

The total area was divided into 5 zones, each of which was further divided into smaller areas, varying in number from 3 to 6. The size of the individual areas varies between 8 and 12 hectares, although there are exceptions determined by the morphology of the area to be surveyed.

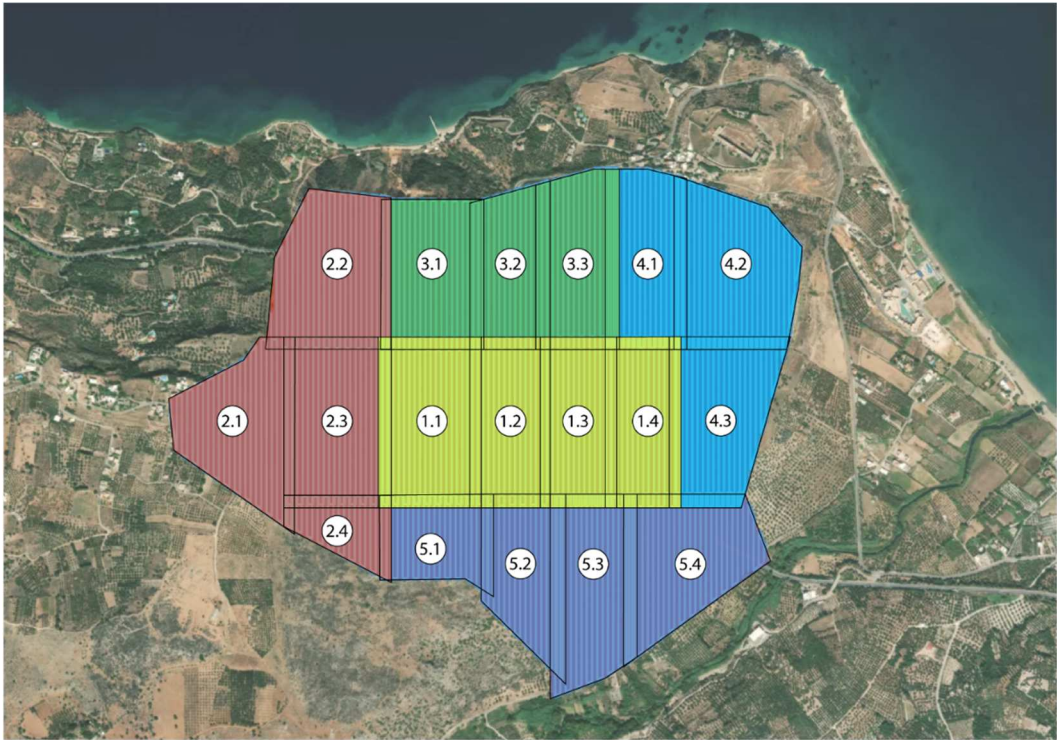


Figure 6. Initial flight strategy.

The flight altitude was determined based on the desired spatial resolution, expressed by the Ground Sampling Distance (GSD). The GSD is the distance, measured on the ground, between two adjacent pixels in the image. For the present study, the desired GSD is about 2 cm/pixel, therefore the flight altitude was identified at an altitude of approximately 40-50m.

However, the Premium plan does not allow the flight altitude to be set as a variable function relative to the ground but as a constant function relative to the “home” point, which makes the definition of flight altitude dependent on the altitude of the starting point and the resulting GDS variable according to the morphology of the surveyed area. Moreover, it should be noted that, as the workshop's focus was on surveying the upper and predominantly flat area of the plateau, the altitudes and the GDS refer to the average elevation of this area, to the detriment of the quality of sloping areas or at the foot of the plateau that can descend up to 150 meters in elevation, but which do not constitute the primary objective of the work.

The vertical overlap between shots and the lateral overlap between strips was set at 75% to ensure a larger safety margin. Although a reduction in overlap would have resulted in time and battery



savings, it would have compromised the safety of the area's survey coverage, which was not considered acceptable given the time constraints required by the workshop.

The different areas overlap by about 40 meters, equivalent to about 2 stripes, to ensure continuity in the photo processing process and prevent any gaps in the image.

The UAV speed was set at the default value of 16.1 km/h to avoid flying too quickly and obtaining blurry photographs.

The average extent of each area, around 10 hectares, was deemed optimal considering the limitation of not exceeding a maximum distance of 1.5 km between the operator and the drone for safety reasons.

Below is a schema that summarizes the defined input parameters and the output results obtained from Dronelink's "Mission Preview" function, in terms of completion time, batteries used, and resulting GSD with respect to the home point, based on the entered data.

**Table 1.** Initial flight strategy.

Zone	Area	hectares	Altitude(m)	Flight duration	N° batterires	GSD (cm/pix)
1	1	12.1	40	00:36:40	9	1.42
	2	9.7	40	01:06:47		1.42
	3	9.0	40	01:33:20		1.42
	4	9.3	40	02:01:46		1.42
2	1	11.1	40	00:37:40	9	1.42
	2	12.3	40	01:15:20		1.42
	3	12.8	40	01:52:56		1.42
	4	4.3	40	02:09:54		1.42
3	1	10.4	40	00:33:16	7	1.42
	2	9.0	40	01:00:04		1.42
	3	10.1	40	01:32:25		1.42
4	1	9.9	40	00:32:07	8	1.42
	2	12.9	40	01:12:48		1.42
	3	11.0	40	01:47:04		1.42
5	1	7.0	40	00:21:35	7	1.42
	2	9.1	40	00:43:21		1.42
	3	11.4	40	01:12:38		1.42
	4	11.8	40	01:44:32		1.42

Please note that, in the absence of a precise indication of wind strength, the software's estimated duration of battery life is 15 minutes.

### 2.3.3. Executed Flight plan

The flight plan prepared a priori proved to be fairly consistent with the situation found on site, despite the need for some modifications and the exclusion of some areas for reasons of force majeure. In particular, it was confirmed that the planned altitude settings could be maintained, as there were no poles or pylons in the vicinity.

However, the main problem was the impossibility of entering certain areas due to private property or prohibitive morphological conditions. Therefore, it was necessary to reduce the area covered by the survey and exclude some areas due to the too high distance that would be created between the operator and the UAV, considering possible signal losses and the obstructive action of the wind with respect to the control of the UAV. In general, distances greater than 1.5 km from the operator were avoided, as at these distances the signal was fluctuating and the energy consumption of the battery became too high compared to the promised effectiveness.

Below is a diagram representing the areas that were actually surveyed.

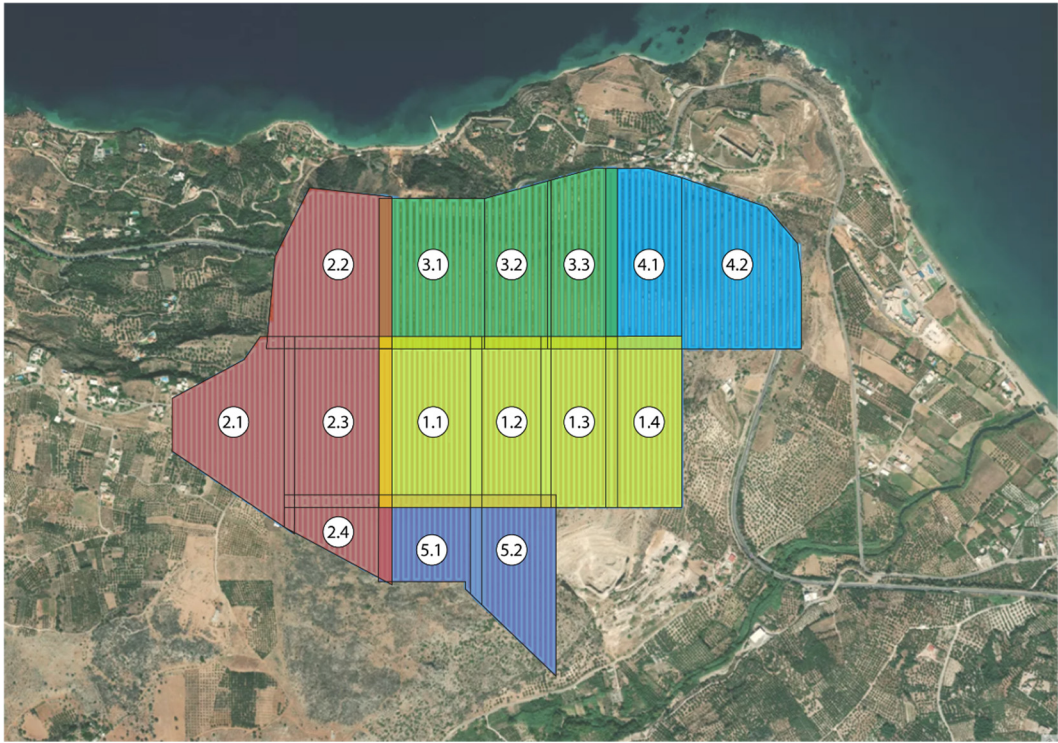


Figure 7. Executed flight strategy.

Below, the changes made to flight parameters and area extensions are being discussed.

Table 2. Executed flight strategy.

Zone	Area	hectares	Altitude(m)	Flight duration	Nº batterires	GSD (cm/pix)
1	1	12.1	40	00:36:40	9	1.42
	2	9.7	40	01:06:47		1.42
	3	9.0	40	01:33:20		1.42
	4	9.3	40	02:01:46		1.42
2	1	11.1	40	00:35:34	9	1.42
	2	12.3	40	01:14:03		1.42
	3	12.8	40	01:54:42		1.42
	4	4.3	40	02:09:06		1.42
3	1	10.9	50	00:27:54	5	1.78
	2	7.7	50	00:47:32		1.78
	3	9.0	50	01:09:55		1.78
4	1	9.6	50	00:24:26	4	1.78
	2	8.3	55	00:53:23		1.96
	3	-	-	-	-	-
5	1	6.4	40	00:22:05	4	1.42
	2	8.3	40	00:47:20		1.42
	3	-	-	-		-
	4	-	-	-		-

The extent of the areas and zones defined in the first approach phase was consistent with the objectives of field survey efficiency and digital reconstruction effectiveness in the office, except for some aspects of overlapping areas that could be optimized. The overlap between adjacent areas set at 40m in the first flight hypothesis was indeed slightly redundant in the post-first campaign processing phase: an overlap of 20 meters, equivalent to about the area swept by a stripe, would have been sufficient, even in terms of safety coverage. For this reason, and for the usual reasons of time

and battery savings, the adjacent areas belonging to zones 4 and 5 were surveyed by overlapping a single stripe between their paths (e.g. areas 3.1-3.2.3.3 and 4.1-4.2).

To avoid being too far from the drone, the UAV's starting (and return) point was moved with each battery change, trying to center as much as possible in the area to be surveyed. It was noted that the maximum distance of 1.5 km represented the limit beyond which the signal could regularly be lost, albeit momentarily.

After the first processing of the images, the quality achieved was found to be satisfactory, so it was decided to confirm the flight altitudes and possibly raise them for the benefit of the acquisition times (e.g. zones 3), provided that any additional altitude variations were made in the case of significant average altitude variations within the area compared to the starting/return point (e.g. zone 4).

The vertical overlap between shots and lateral between strips was deemed satisfactory based on the first digital reconstructions and for this reason it was maintained as previously indicated.

The UAV speed of 16.1 km/h proved to be adequate for the purposes of the survey, although less favorable when returning home (RTH) due to the large distance from the home point at low speed, which involved a significant battery consumption. Despite this, it was decided to maintain this speed and, if necessary, to manually manage the return home without incurring, in this way, the speed limits of the automatic flight.

Finally, we end the report on the actual estimates of time and battery consumption: in general, the estimates were respected, with an autonomy of about 15-20 minutes per battery, except in the acquisition phases where the wind was blowing stronger, reducing battery life and consequently increasing the actual survey time.

#### 2.4. GNSS survey

As previously mentioned, to optimize photogrammetric reconstruction and georeference the final models, it is essential to use the geographical coordinates obtained through GNSS surveying, referred to a specific reference system.

GNSS (Global Navigation Satellite System) is a measurement technique based on the use of satellites (such as GPS, GLONASS, Galileo, and BeiDou) to determine the precise position of a point on the earth's surface. GNSS receivers receive signals from satellites and calculate the coordinates in a global reference system. To convert these coordinates into a specific system, such as WGS84, coordinate transformations are applied. Various software and online tools are available to facilitate these conversions and transformations.

The points surveyed via GNSS surveying can be distinguished into two types: Ground Control Points (GCPs) and Quality Check Points (QCPs). The coordinates of the GCPs are used to orient, scale and georeference the three-dimensional model derived from the photogrammetric processing; instead, the coordinates of the QCPs (surveyed in the field) are used to see how much they deviate from the coordinates of the same points processed by the software and returned and are therefore used to define the accuracy of the resulting DEM model.

##### 2.4.1. GNSS instruments

For the GNSS survey, a CHCNAV i73 antenna was used, which includes RTK and IMU capabilities, kindly lent by the Senselab Space Informatics office of the Technical University of Crete.

RTK (Real-Time Kinematics) technology for GNSS poles is an advanced and highly accurate system for real-time positioning, used in a wide range of applications where precision is essential, ensuring millimetric accuracy and thus proving to be a valuable tool for surveyors. The method involves the base receiver recording satellite signals and calculating the exact position of the reference station, then transmitting this information to the rover receiver in real time. The rover receiver uses this information to calculate its exact position.

The acronym IMU stands for Inertial Measurement Unit. In the context of surveying and construction, the combination of IMU with GNSS allows new smart antennas functionalities, including measuring without calibration with a misaligned pole and insensitivity to electromagnetic fields. The

smart antenna with integrated IMU allows measurements to be taken without aligning the pole with a high tilt even of 60°.

#### 2.4.2. GCP survey plan

Initially, an optimal planning for the positioning of GCP and QCP was thought, considering to position the GCP at a distance of 150-200m and some QCP in a random manner. However, this a priori planning proved to be too optimistic at the time of implementation. In addition to time issues dictated by workshop times, logistical difficulties emerged such as the lack of transport means within the site, the inability to access private areas and to move outside the beaten paths due to the morphology of the plateau.

Furthermore, since no photogrammetric targets were available, it was necessary to survey morphological points recognizable from a height of 40 meters, thereby compromising the precision of the reconstruction operation.

Possible integrations of GNSS data will be evaluated in the future, if necessary. The recovery of this information is not excluded, but in the context of this workshop and with the above-mentioned problems, it was preferred to focus on aerial photogrammetric survey ensuring a maximum georeferencing of the models and postpone any denser GNSS surveys in the future, in order to obtain a more precise and accurate reconstruction of the outputs created here.

For these reasons, only 10 points belonging to the upper plane of the plateau, corresponding to the archaeological site, were surveyed, while it would have been preferable to also survey some points at the foot of the plateau to ensure a more reliable coverage of the entire landscape.

Since the quantity of points surveyed is very limited for such a territorial scale, for the purpose of reconstructing the model of the entire plateau all surveyed points will be considered GCP and no QCP will be used. This procedural choice, forced by reasons of force majeure, will not allow to study the degree of accuracy of the associated digital reconstruction.

However, with the aim of not neglecting the analysis of accuracy, it was decided to circumscribe the aforementioned analysis to the heart of the archaeological site, focus of the workshop, located in the upper part of the plateau, where it was possible to collect an adequate number of reference points and for which a detail model will be created.

To summarize the methodological choice made and introduce the next work phases, in the next chapters will be presented:

- the procedural phases for the generation of DEM and DEM-TIN models, orthophotos and contour lines, through the SfM Metashape software, with the aim of creating the digital models of both the entire plateau and the archaeological site in particular;
- the study on the accuracy and quality of the results obtained, concentrated on the area of the archaeological site.

#### 2.5. Photogrammetric data processing

At the end of each day of field data collection, once we returned to the office, the focus shifted to the data processing phase. This essential step allowed to verify the quality of the information collected in the field and to provide the working teams involved in the workshop with fundamental material, such as point clouds, meshes, DEMs and orthophotos, in a very short time, for their daily commitment.

For the photogrammetric reconstruction activity, Agisoft Metashape software was used.

In this chapter, it will be presented the workflow used to generate the typical outputs for a digital reconstruction project of a territorial-scale object.

In the next chapter, instead, we will focus on the analysis of the quality and accuracy of the results obtained: as already mentioned, for this second purpose we will examine a smaller area within the same plateau, for which the same workflow that we will expose in the next paragraphs was followed.

Below, it is presented a brief summary of the phases of the reconstruction process that we will soon discuss in more detail:



- Photo alignment
- GCP and QCP definition
- Alignment optimization
- Dense cloud
- Point classification
- 2D-DEM (DTM)
- Contour lines
- DSM-TIN and DTM-TIN (Mesh with texture)
- Orthomosaic

#### 2.5.1. Photo alignment

The first step in our process involved importing the 8532 photos acquired, organized into folders corresponding to individual missions. Subsequently, we estimated the camera positions using the “Align Photos” command.

The parameters and values used are as follows:

- Accuracy: High
- Generic preselection: yes
- Referece preselection: yes, Source
- Reset curent alignment: -
- Key point limit: 40.000
- Tie point limit: 4.000
- Apply mask to: none
- Exclude stationary tie points: no
- Guided image matching: no
- Adaptive camera model fitting: yes

Higher accuracy settings help to obtain more accurate camera position estimates. Lower accuracy settings can be used to get the rough camera positions in a shorter period of time. In the Generic preselection mode, the overlapping pairs of photos are selected by matching photos using lower accuracy setting first, benefiting the processing time. In the Source preselection mode, the overlapping pairs of photos are selected based on the measured camera locations (in this case, the GPS position present in the metadata of the drone photos). Key point and Tie point limit were indicated as recommended by the Metashape guide. Adaptive camera model fitting helps to prevent the divergence of some parameters for datasets with weak camera geometry, like a typical aerial dataset.

At this stage, it is possible to explore the Tie Points and observe, as indicated in blue in the following image, the positioning of the cameras.

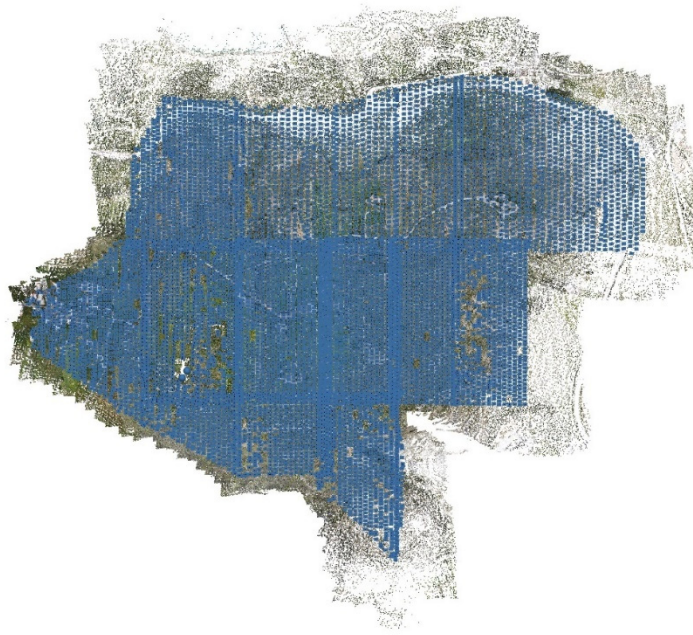


**Figure 8. Tie points and camera locations.**

Subsequently, the 10 detected points from the GNSS antenna were identified by placing their respective markers in all the photographs where those points were present.



**Figure 9. Tie points and markers identification.**

The next step involved georeferencing the model by importing the point coordinates into Metashape.

Firstly, the reference system was modified from the default WGS84 (EPSG::4326) to WGS84 (EPSG::32635) which corresponded to the system of the point coordinates obtained through GNSS. Subsequently, the camera information was automatically converted by selecting the appropriate option.

**Table 1.** GNSS survey – points coordinates.

Marker	Easting (m) - survey	Northing (m) - survey	Altitude (m) - survey
1	512663,286	3924086,250	217,233
2	512680,138	3924117,120	213,147
3	512665,874	3924204,077	205,814
4	512699,736	3924220,669	203,286
5	512747,623	3924166,389	206,227
6	512748,647	3923848,650	211,528
7	512506,672	3923891,421	218,460
8	512390,339	3924087,504	219,545
9	512654,232	3924270,943	208,973
10	513234,929	3924361,905	192,365

Subsequently, the corresponding .csv file was loaded using the “Import Reference” command, and the Markers were automatically updated with the coordinates from the file.

At this point, we moved on to the alignment optimization phase.

The GPS information associated with the drone-derived cameras was deactivated as it was not desired to use them as a reference for alignment optimization due to their lower reliability compared to the newly inserted GPS coordinates.

Markers to be used for optimization were then selected, distinguishing between GCPs (Ground Control Points) and QCPs (Quality Control Points). For the entire plateau model, due to the lack of GCPs, all Markers were used as GCPs. However, for the detailed model used in the accuracy analysis chapter, as will be seen, various combinations of GCPs and QCPs were tested to study different results.

In the reference settings panel, the assumed accuracy of the measured values was specified (0.005m). The “Optimize Camera Alignment” command was used to further refine parameters related to the photographic data.

Once completed, the new camera alignment was defined, and new tie points were created.

It is now possible to proceed to the next phase: generating the dense point cloud.

#### 2.5.2. Dense point cloud generation and management

In order to achieve a good result in a timely manner, the dense point cloud was generated with the following settings:

Dense cloud generation:

- Quality: Medium
- Depth filtering: Mild
- Calculate point colors: yes
- Calculate point confidence: yes

This resulted in a point cloud consisting of 256,572,086 points.



**Figure 10.** Dense point cloud generated.

Subsequently, the “Filter by Confidence” command was used to assess the point cloud created in terms of confidence. This function allows filtering points within a confidence range defined by the user, which can range from 0 to 255. It was decided to remove points with values in the range from 0 to 2.

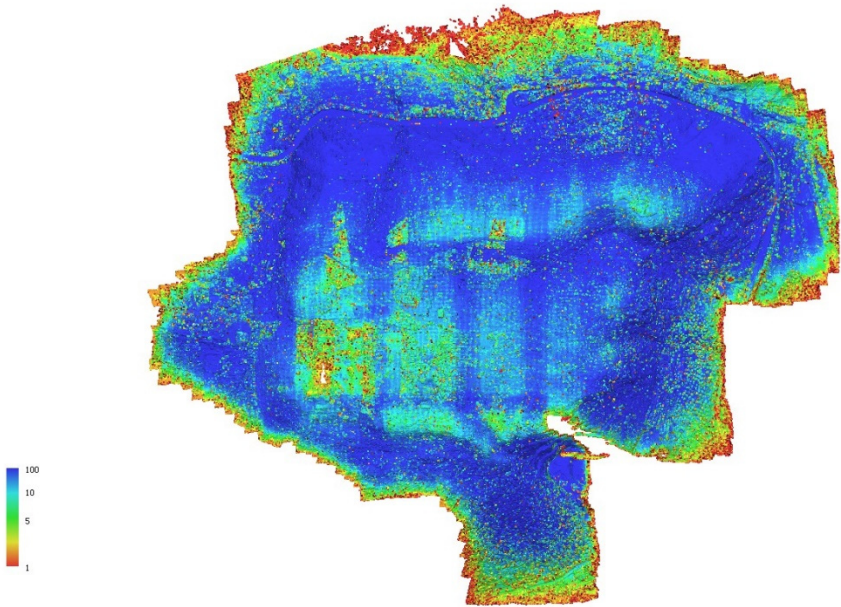


**Figure 11.** Dense point cloud – confidence level classification.



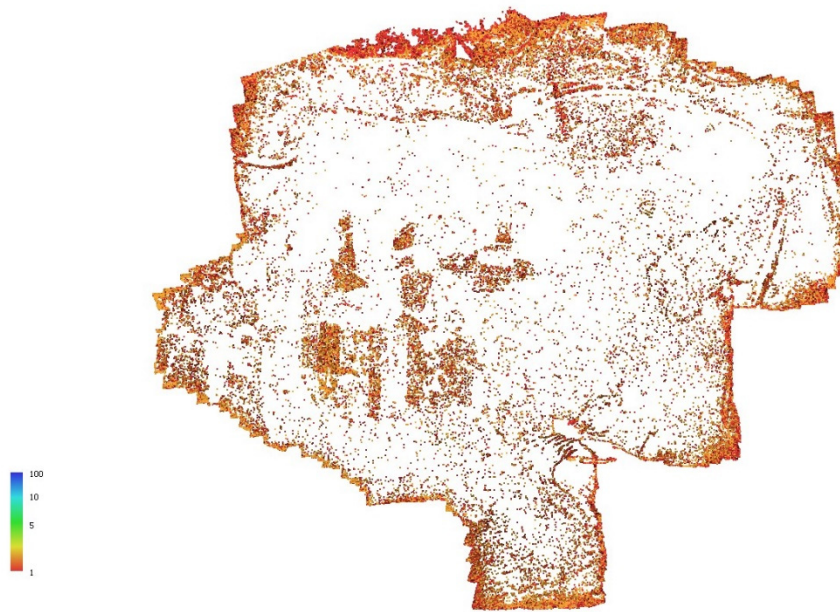


**Figure 12.** Dense point cloud – 0-2 range confidence.

As a result, the number of points in the point cloud decreased from 256,571,864 to 213,416,628, which represents approximately 80% of the original number.

To obtain a Digital Terrain Model (DTM), it is now necessary to classify the point cloud and remove points that do not represent the terrain, such as vegetation, man-made objects, water bodies, etc. The Metashape software provides options for manual or semi-automatic point classification, allowing for iterative refinement of the process by manipulating key parameters.

1. Classify ground points.

A semi-automatic method that allows the recognition of only ground points through the definition of values for 4 parameters is as follows:

- a. Max angle (deg): sets limitation for an angle between terrain model and the line to connect the point in question with a point from a ground class.
- b. Max distance (m): sets limitation for a distance between the point in question and terrain model.
- c. Cell size (m): Determines the size of the cells for point cloud to be divided into as a preparatory step in ground points classification procedure.
- d. Erosion radius (m): determines the indentation (in meters) from unclassified points, ground points within that area will be unclassified.

2. Classify points.

Another semi-automatic method that allows for classifying points into different categories (including an uncategorized category) by defining a confidence value ranging from 0 to 1.

The categories include:

- a. Ground
- b. High vegetation
- c. Building
- d. Road surface
- e. Car
- f. Man-made object

3. Assign class:

A manual method that allows for selecting points of interest and modifying their class. This can be a valuable support to semi-automatic classification to quickly correct the classification of specific areas that were not properly classified by the software.

The classification workflow consisted of multiple phases:

1. Ground point classification.

Through an iterative method, values were determined that allowed for an initial satisfactory classification of the point cloud.

- a. Max angle (deg): 15
- b. Max distance (m): 0.05
- c. Cell size (m): 20
- d. Erosion radius (m): 0

The point cloud was then classified into the following categories:

- a. Unclassified points (grey)
- b. Ground points (brown)
- c. Low noise points (pink)

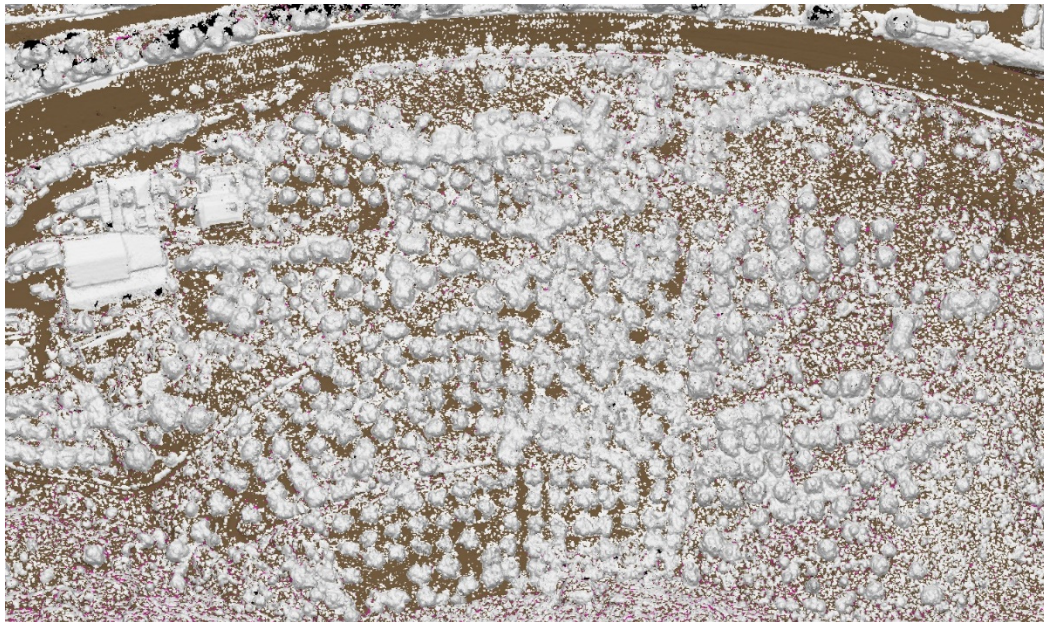


**Figure 13.** Detail view of the ground classification result.

2. Assign points.

Some points that clearly belonged to the “ground points” category were not included. Therefore, these points were selected and their classification was manually set. Among these points, for example, there were some rocks that the software may have mistaken for trees, bushes, man-made objects, or background noise.





**Figure 14.** Manual points classification.

3. Classify points.

Before proceeding to the second phase of classification, it was necessary to reset the existing classification to avoid the “wrong point count” error. This operation was performed after removing points classified and confirmed as non-ground, preserving and refining the previous work. As a result, the number of points in the point cloud decreased from 213,416,628 to 101,715,919.

Subsequently, the “classify points” operation was executed. After a series of iterative tests, it was determined that a confidence value of 0.7 was appropriate. The classification was limited to the “ground” and “high vegetation points” classes, with the goal of refining the classification of the terrain point cloud by removing further vegetation components. Points belonging to the “high vegetation” category were then eliminated, resulting in a reduction of the point cloud from 101,715,919 to 93,193,523 points.

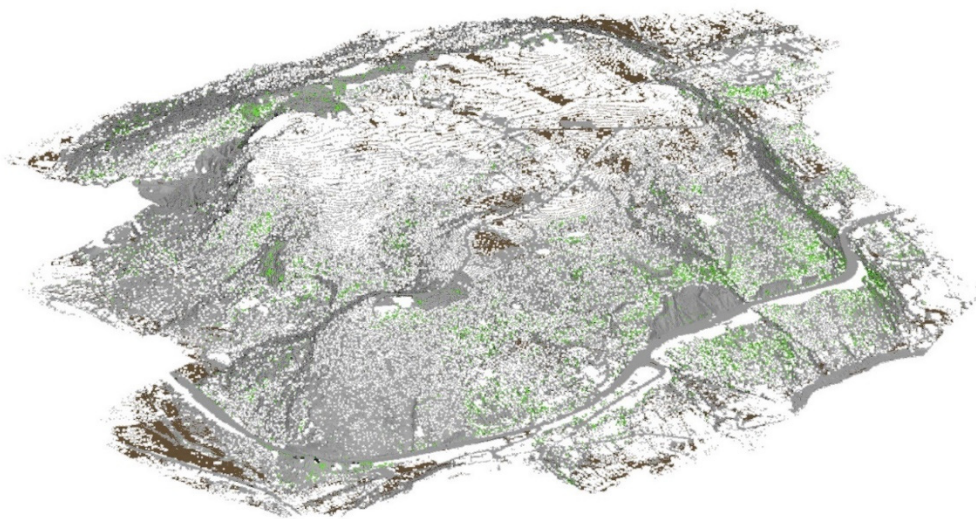


**Figure 15.** Point cloud classification.

#### 4. Assign points.

At this stage, all the remaining points were manually reclassified as “ground points.” Finally, some less significant outlier points were removed from the point cloud. As a result, the number of points in the point cloud decreased from 93,193,523 to 87,865,204. Therefore, compared to the initial point cloud, the final point cloud contains 34% of the starting points.

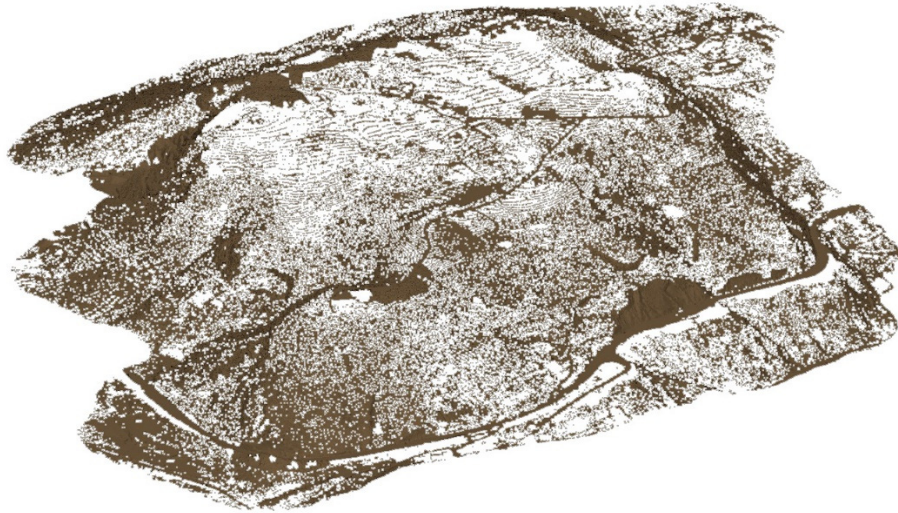


**Figure 16.** Definitive ground points classification.

#### 2.5.3. DEM-2D (DTM) generation

At this point, we proceeded with the creation of the two-dimensional Digital Terrain Model (DTM). To achieve this, we selected the newly created terrain point cloud model and executed the “Build DEM” command.

The following are the parameters and values used:

- Projection type: Geographic, GGRS87
- Source data: Dense cloud
- Interpolation: Enabled (default)
- Point classes: Ground
- Resolution: 0.111829 (not editable)
- Total size (pix): 27936x21837



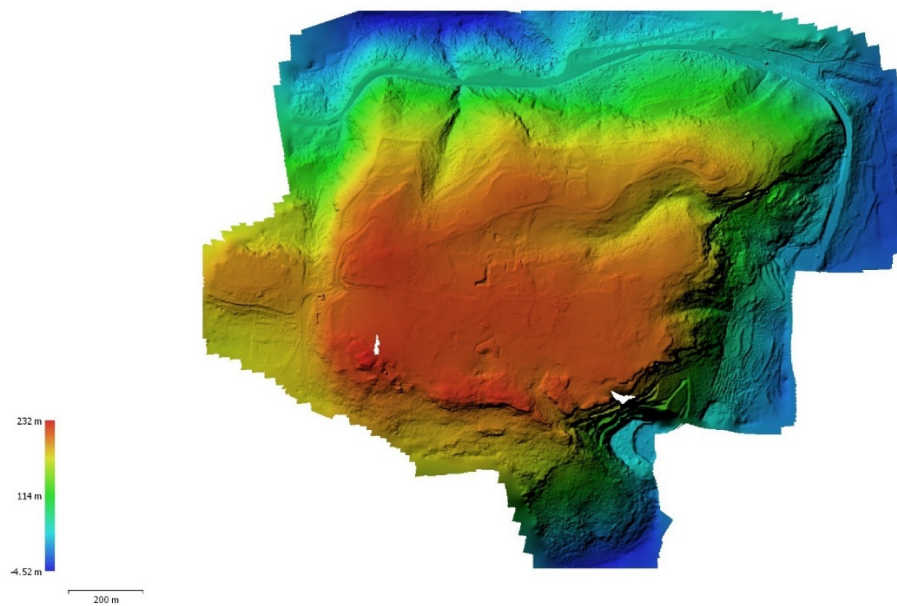


Figure 17. 2D-DTM model.

#### 2.5.4. Contour lines generation

Using the produced DEM, contour lines of the model can now be generated with the “Generate contours” command.

The following parameters were set for this purpose:

- Source data: DEM
- Min altitude (m): -4.52
- Max altitude (m): 231.70
- Interval (m): 10 or 1
- Prevent intersections: yes

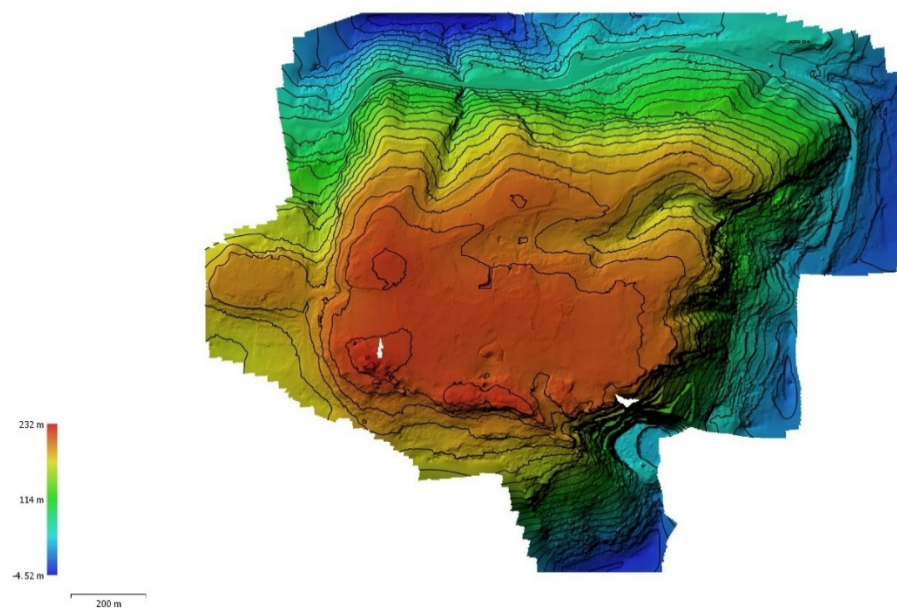


Figure 18. 2D-DTM model with contour lines (10m interval).

### 2.5.5. DEM-TIN (DSM and DTM) generation

The DEM-TIN models for both the DSM and DTM were created using the “Build mesh” command to construct the geometry and the “Build texture” command to apply color data.

For the DEM-TIN model of the DSM, the following parameters and values were set:

- Source data: Dense cloud (the optimized point cloud model based on confidence)
- Surface type: Arbitrary (3D)
- Quality: -
- Face count: Medium (23.000.000)
- Interpolation: Enabled (default)
- Depth filtering: -
- Point classes: All
- Calculate vertex colors: No
- Use strict volumetric masks: -
- Reuse depth maps: -

A mesh consisting of 26,452,815 faces was then generated. For the DEM-TIN model of the DSM, the following parameters and values were set:

- Source data: Dense cloud (the final DTM point cloud model)
- Surface type: Height field (2.5D)
- Quality: -
- Face count: Medium (5.857.860)
- Interpolation: Enabled (default)
- Depth filtering: -
- Point classes: All
- Calculate vertex colors: No
- Use strict volumetric masks: -
- Reuse depth maps: -

A mesh with 5,769,130 faces was generated. The mesh was then cleaned in the outer areas, resulting in 5,700,490 faces.



**Figure 19.** Comparison: DSM model detail.



**Figure 20.** Comparison: DTM model detail.

Lastly, the texture was generated, using identical parameters for both the DTM and DSM models:

- Texture type: Diffuse map or Occlusion map
- Source data: Images
- Mapping mode: Generic
- Blending mode: Mosaic (default)
- Texture size/count: 8000x8 or 16000x1
- Enable hole filling: yes
- Enable ghosting filter: no



**Figure 21.** DTM (TIN) model with diffuse map texture.

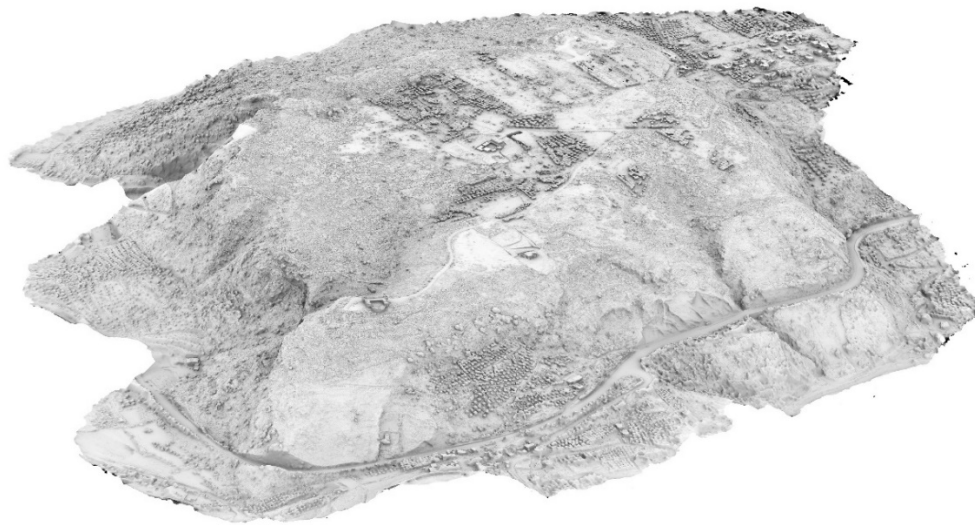


**Figure 22.** DSM (TIN) model with occlusion map texture.

#### 2.5.6. Orthomosaic generation

Finally, an orthomosaic of the plateau was created using the “Build orthomosaic” command. The following settings and parameters were applied:

- Projection Type: Geographic – GRS87 (EPSG::4121)
- Surface: Mesh DTM (2.5D)
- Blending mode: Mosaic
- Refine seamlines: no
- Enable hole filling: no
- Enable ghosting filter: no
- Enable back-face culling: no
- Pixel size (m): 3 cm/pix

At the “surface” option, you can choose between Mesh or DEM. However, the results demonstrate that the 2.5D Mesh provides better image projection onto the surface compared to DEM.



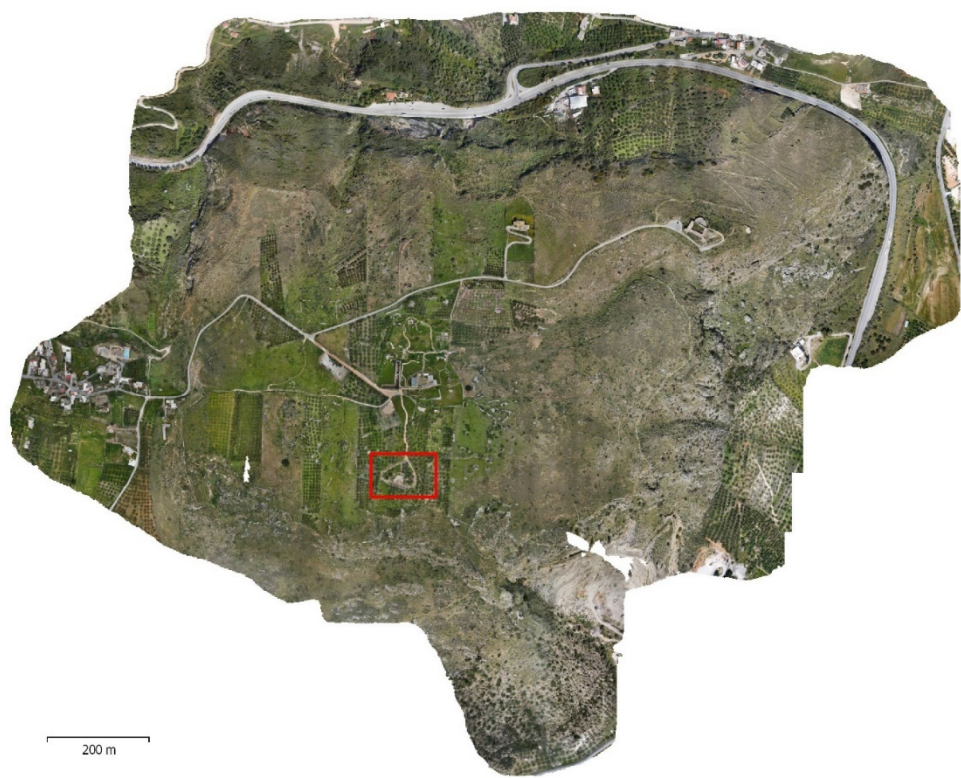


Figure 23. Orthomosaic.



Figure 24. Orthomosaic detail 1.



**Figure 25.** Orthomosaic detail 2.

#### 2.6. Standards for accuracy analysis:

The quality and accuracy of DTM results depend on various factors that can be grouped into four categories [19]:

- **Area characteristics:** This includes the size and morphology of the area, types of ground cover-age, lighting conditions (e.g., cloudy weather), and color contrast of objects.
- **UAV data collection systems:** Factors such as the characteristics of the UAV data collection sys-tem, including the camera and its calibration, and the type of platform used (multicopter or fixed wing), which may have a survey-grade GNSS/RTK receiver.
- **Data acquisition and flight parameters:** Parameters such as flight altitude and configuration, im-age overlap, UAV flight speed, flight path pattern (single or double grid), acquisition of images from the nadir or oblique angles, and the number and distribution of Ground Control Points (GCPs).
- **SfM approaches and ground filtering algorithms:** This category relates to the methods used for Structure from Motion (SfM) and the algorithms employed to automate ground filtering from the 3D point cloud.

To evaluate the accuracy of a 3D point cloud, three different methods can be employed, where the data are typically compared to a more accurate independent source [19]:

- **Method 1:** Analyzing the residuals from the bundle adjustment once the 3D model is rotated and scaled. This method does not require or use independent measurements and should be as-sessed in terms of internal precision rather than accuracy.
- **Method 2:** Comparing the coordinates of the 3D model with Quality Control Points (QCPs).
- **Method 3:** Analyzing the residuals of the 3D model compared to a reference surface obtained using another technique (e.g., TSL). This method is relatively expensive but can be useful for comparing techniques in a specific application.

In the section 3.2, we will evaluate the accuracy of the case study using methods 1 and 2. To facilitate this evaluation, we introduce an important metric commonly used in accuracy studies, namely the Root Mean Square Error (RMSE). The RMSE can be calculated along a specific axis (x, y, or vertical z) or within a plane (horizontal r).



$$RMSE_x = \sqrt{\frac{\sum_i^n (xc_i - xv_i)^2}{n}}, \quad (1)$$

$$RMSE_y = \sqrt{\frac{\sum_i^n (yc_i - yv_i)^2}{n}}, \quad (2)$$

$$RMSE_z = \sqrt{\frac{\sum_i^n (zc_i - zv_i)^2}{n}}, \quad (3)$$

$$RMSE_r = \sqrt{RMSE_x^2 + RMSE_y^2}, \quad (4)$$

where:

- $RMSE_x$ ,  $RMSE_y$ , and  $RMSE_z$  are the root-mean-square error in x, y and z, respectively;
- $RMSE_r$  is the horizontal root-mean-square error;
- $xc_i$ ,  $yc_i$ , and  $zc_i$  are the coordinates of the  $i^{th}$  CP in the dataset;
- $xv_i$ ,  $yv_i$ , and  $zv_i$  are the coordinates of the  $i^{th}$  CP in the independent source of higher accuracy;
- $n$  is the number of check points tested;
- and  $i$  is an integer ranging from 1 to  $n$ .

The lower the RMSE value is, the more accurate the DEM.

It should be noted that in various studies, also other accuracy indicators have been utilized, such as standard deviation, mean error, mean absolute error, or linear regression [2].

Finally, we introduce an important accuracy standard, the ASPRS (American Society for Photogrammetry and Remote Sensing) standard, which is based on the Root Mean Square Error (RMSE).

The ASPRS standard, widely adopted and recognized in UAV photogrammetry studies, defines both horizontal and vertical accuracy. The horizontal accuracy is determined through RMSE statistics in non-vegetated terrain, while the vertical accuracy is assessed using 95th percentile statistics in vegetated terrain [2].

Corresponding accuracy estimates at the 95% confidence level are calculated using NSSDA (National Standard for Spatial Data Accuracy) methodologies, as described by Equations (8)-(10).

$$Accuracy_r = 1.7308 \times (RMSE_r), \quad (5)$$

$$Accuracy_z [NVA] = 1.96 \times (RMSE_z), \quad (6)$$

$$Accuracy_z [VVA] = 3 \times (RMSE_z), \quad (7)$$

where  $Accuracy_r$  is the horizontal accuracy at the 95% confidence level;  $Accuracy_z$  is the vertical accuracy at the 95% confidence level; NVA means non-vegetated terrain; and VVA means vegetated terrain (VVA) [2].

### 3. Results

#### 3.1. Subsection

The work carried out has led to the generation of various types of output that can be used by workshop participants in various ways.

In particular, through exporting from Metashape, the following outputs were delivered:

- Dense point clouds: exported in \*e57 open format. These were primarily used as a record of the surveying work and for creating evocative images of the archaeological site. Views were captured through the appropriate command within Autodesk Recap, a software for managing the point cloud that is intuitive and useful for studying the cloud using bounding box, measurement, point visibility and color management, screenshot, and annotation functions. In order to

not have to proceed more than once with the lengthy import of the \*e57 file into Recap, a \*rcs point cloud model was also created (Autodesk proprietary).

- Textured DTM/DSM meshes: exported in \*obj format for geometry, \*jpg for texture image, \*mtl for geometry-texture correlation. The mesh models represent the most manageable and exploitable output for three-dimensional project analysis and details. The DTM can be used in particular to extract environmental morphological sections, while the DSM carries three-dimensional information concerning also the vegetation and buildings present in the archaeological site. Two types of textures were generated: diffuse map and occlusion map. The “diffuse map” type presents color data from the mosaicking of image projections while the “occlusion map” type presents a grayscale color data from ambient occlusion. The diffuse map gives a suggestive realistic effect to the model, while the occlusion map highlights its geometries. To accommodate various solutions, these types of textures were created in two forms: a higher definition one (8000x8000pix with 8 textures) and a lower one (16000x16000pix with 1 texture). The obj format is manageable through different software, within the workshop the most used were Rhinoceros3D and Sketchup.
- Contour lines: exported in \*dxf format. The contour lines, which are vector in nature, were used to represent the terrain's slope in plan in the two-dimensional CAD drawings.
- Orthomosaic: exported in \*tiff format. The orthomosaic represents the main two-dimensional raster output of the work. During export from metashape, it is possible to define the pixel size of the image (cm/pix, 3 in this case, as per orthomosaic generation), the total dimensions (36947x29437 pix, in this case, data derived based on the size of the model and the pixel size defined previously), the possibility of including the alpha channel, the background color, the creation of a Word file with associated metadata, the level of compression, etc... A great possibility of the \*tiff is that it can be imported onto CAD at a 1:1 scale. The orthomosaic is particularly useful as a background for CAD drawings, to trace specific elements in nadir view or as a project masterplan or various detail documents.

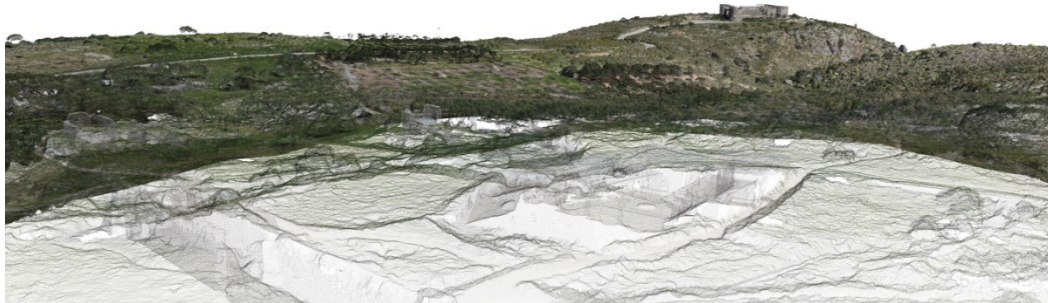


**Figure 26.** Evocative view of the 3D point cloud.

### 3.2. Accuracy analysis

In this paragraph, the focus will be on the accuracy analysis of the digital terrain model.

As mentioned in section 2.4.2, the topographic survey was conducted with a limited number of GPS points, mainly concentrated on the main archaeological site for a specific project. Therefore, it has been decided to analyze the digital model within the larger contextual area, which measures 525x490m. To achieve this, the 1898 cameras related to the area were selected, and a new Metashape project was created using these cameras.



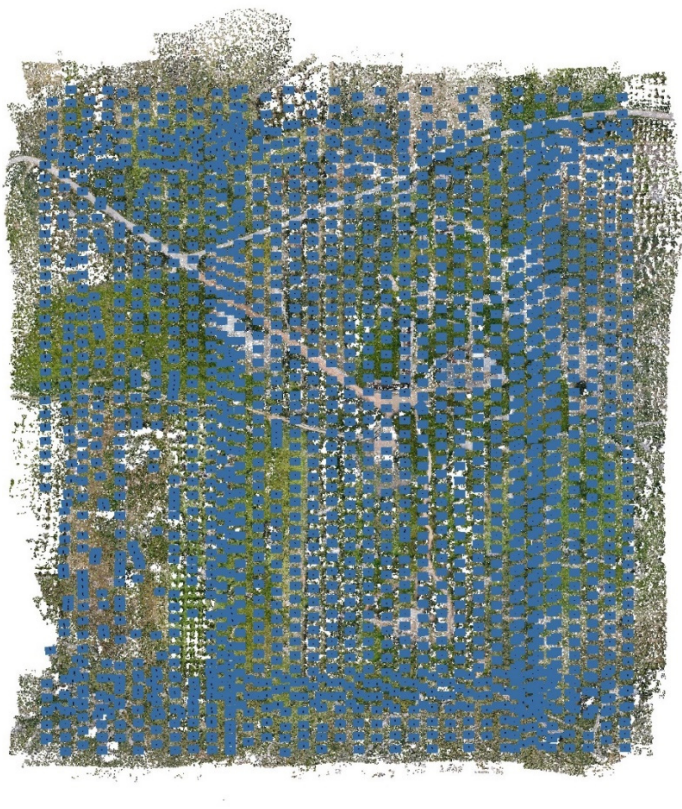


**Figure 27.** Tie points and camera locations.

As observed previously, the cameras were aligned, tie points were generated, and the GPS points were accurately identified through their respective markers (9 out of the total 10 detected). Their accurate identification was achieved in all the images where they are present.



Figure 28. Tie points and markers identification.

At this stage, a different approach was taken compared to what was done in chapter 2.5, where all the GPS points detected were used as GCPs. The tie points were duplicated eight times, in order to create multiple models to analyze different combinations of GCPs and Quality Control Points (QCPs).

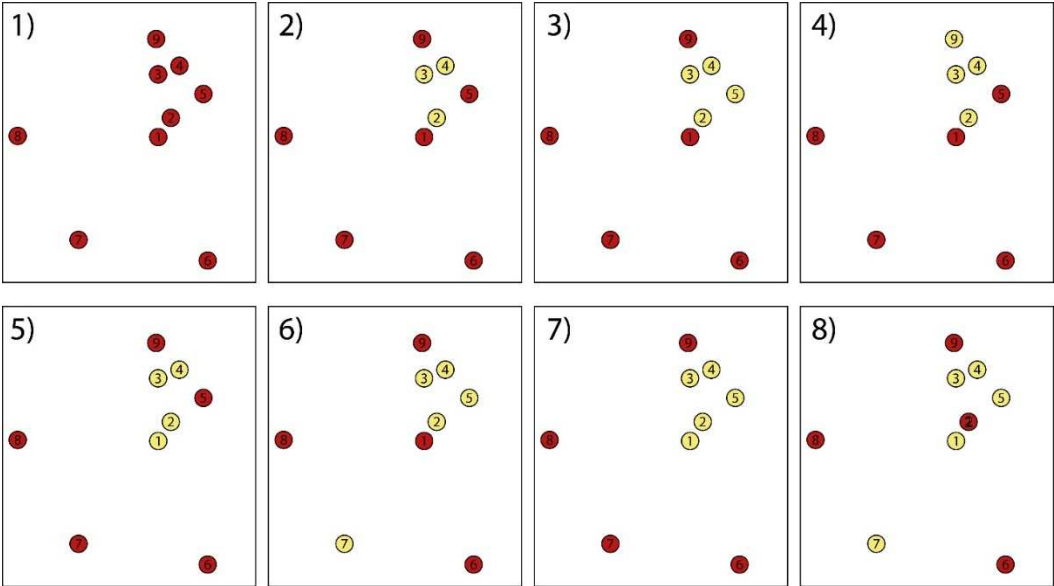


Figure 29. GCP (red) and QCP (yellow) combinations.

For each of these models, the alignment of the cameras was optimized based on the respective GCPs. The accuracy of the corresponding QCPs was then analyzed using method 2 outlined in chapter 2.6.

Method 1, on the other hand, was only used in cases where all nine markers were used as GCPs. As mentioned before, it is more appropriate to discuss the precision of the model in this scenario rather than accuracy. The interpretation of the analysis result differs from that of method 2 cases, and this will be explained in more detail in chapter 4.

Below is a table displaying the initial data and the accuracy values obtained for each combination. The initial data was exported using the appropriate “Export reference” command.

Table 1. Accuracy assessment strategy: survey and digital model coordinates.

Accuracy assessment strategy				Survey coordinates			Digital model coordinates		
Combina- tion	Marker	GCP	QCP	Easting x <sub>vi</sub> (m)	Northing y <sub>vi</sub> (m)	Altitude z <sub>vi</sub> (m)	Easting x <sub>ci</sub> (m)	Northing y <sub>ci</sub> (m)	Altitude z <sub>ci</sub> (m)
1	1	1	1	512663,286	3924086,25	217,233	512663,24	3924086,259	217,221
	2	1	1	512680,138	3924117,12	213,147	512680,124	3924117,127	213,172
	3	1	1	512665,874	3924204,077	205,814	512665,927	3924204,142	205,78
	4	1	1	512699,736	3924220,669	203,286	512699,707	3924220,696	203,321
	5	1	1	512747,623	3924166,389	206,227	512747,457	3924166,393	206,263
	6	1	1	512748,647	3923848,65	211,528	512748,555	3923848,587	211,52
	7	1	1	512506,672	3923891,421	218,46	512506,748	3923891,274	218,454
	8	1	1	512390,339	3924087,504	219,545	512390,463	3924087,524	219,558
	9	1	1	512654,232	3924270,943	208,973	512654,327	3924271,02	208,923
2	1	1	0	512663,286	3924086,25	217,233	512663,261	3924086,281	217,234
	2	0	1	512680,138	3924117,12	213,147	512680,14	3924117,159	213,245

	3	0	1	512665,874	3924204,077	205,814	512665,944	3924204,169	205,747
	4	0	1	512699,736	3924220,669	203,286	512699,708	3924220,713	203,386
	5	1	0	512747,623	3924166,389	206,227	512747,504	3924166,427	206,237
	6	1	0	512748,647	3923848,65	211,528	512748,578	3923848,607	211,529
	7	1	0	512506,672	3923891,421	218,46	512506,72	3923891,312	218,459
	8	1	0	512390,339	3924087,504	219,545	512390,425	3924087,517	219,545
	9	1	0	512654,232	3924270,943	208,973	512654,311	3924271,014	208,963
3	1	1	0	512663,286	3924086,25	217,233	512663,263	3924086,252	217,256
	2	0	1	512680,138	3924117,12	213,147	512680,172	3924117,118	213,443
	3	0	1	512665,874	3924204,077	205,814	512665,95	3924204,108	205,94
	4	0	1	512699,736	3924220,669	203,286	512699,772	3924220,662	203,784
	5	0	1	512747,623	3924166,389	206,227	512747,636	3924166,394	207,043
	6	1	0	512748,647	3923848,65	211,528	512748,636	3923848,65	211,529
	7	1	0	512506,672	3923891,421	218,46	512506,682	3923891,399	218,444
	8	1	0	512390,339	3924087,504	219,545	512390,357	3924087,509	219,555
	9	1	0	512654,232	3924270,943	208,973	512654,239	3924270,958	208,956
4	1	1	0	512663,286	3924086,25	217,233	512663,257	3924086,348	217,256
	2	0	1	512680,138	3924117,120	213,147	512680,17	3924117,221	213,151
	3	0	1	512665,874	3924204,077	205,814	512666,066	3924204,242	204,491
	4	0	1	512699,736	3924220,669	203,286	512699,873	3924220,75	202,099
	5	1	0	512747,623	3924166,389	206,227	512747,597	3924166,419	206,212
	6	1	0	512748,647	3923848,65	211,528	512748,568	3923848,597	211,531
	7	1	0	512506,672	3923891,421	218,46	512506,735	3923891,301	218,451
	8	1	0	512390,339	3924087,504	219,545	512390,412	3924087,549	219,543
	9	0	1	512654,232	3924270,943	208,973	512654,46	3924271,256	206,385
5	1	0	1	512663,286	3924086,25	217,233	512663,247	3924086,301	217,275
	2	0	1	512680,138	3924117,12	213,147	512680,134	3924117,173	213,274
	3	0	1	512665,874	3924204,077	205,814	512665,936	3924204,177	205,753
	4	0	1	512699,736	3924220,669	203,286	512699,699	3924220,72	203,384
	5	1	0	512747,623	3924166,389	206,227	512747,493	3924166,435	206,239
	6	1	0	512748,647	3923848,65	211,528	512748,57	3923848,614	211,529
	7	1	0	512506,672	3923891,421	218,46	512506,716	3923891,317	218,459
	8	1	0	512390,339	3924087,504	219,545	512390,422	3924087,521	219,545
	9	1	0	512654,232	3924270,943	208,973	512654,307	3924271,021	208,962
6	1	1	0	512663,286	3924086,25	217,233	512662,866	3924085,648	216,789
	2	0	1	512680,138	3924117,12	213,147	512679,79	3924116,444	212,857
	3	0	1	512665,874	3924204,077	205,814	512665,654	3924203,407	205,241
	4	0	1	512699,736	3924220,669	203,286	512699,472	3924219,934	203,146
	5	0	1	512747,623	3924166,389	206,227	512747,259	3924165,658	206,611
	6	1	0	512748,647	3923848,65	211,528	512748,045	3923848,072	211,087
	7	0	1	512506,672	3923891,421	218,46	512506,263	3923890,813	216,808
	8	1	0	512390,339	3924087,504	219,545	512390,097	3924087,059	219,024
	9	1	0	512654,232	3924270,943	208,973	512653,992	3924270,221	208,1
7	1	0	1	512663,286	3924086,25	217,233	512663,269	3924086,313	220,17
	2	0	1	512680,138	3924117,12	213,147	512680,188	3924117,164	216,114
	3	0	1	512665,874	3924204,077	205,814	512665,96	3924204,055	207,371
	4	0	1	512699,736	3924220,669	203,286	512699,762	3924220,566	204,909
	5	0	1	512747,623	3924166,389	206,227	512747,624	3924166,372	208,963



	6	1	0	512748,647	3923848,65	211,528	512748,633	3923848,662	211,534
	7	1	0	512506,672	3923891,421	218,46	512506,675	3923891,39	218,45
	8	1	0	512390,339	3924087,504	219,545	512390,35	3924087,515	219,552
	9	1	0	512654,232	3924270,943	208,973	512654,232	3924270,951	208,97
8	1	0	1	512663,286	3924086,25	217,233	512663,224	3924086,25	219,973
	2	0	1	512680,138	3924117,12	213,147	512680,147	3924117,115	215,98
	3	0	1	512665,874	3924204,077	205,814	512665,949	3924204,033	207,303
	4	0	1	512699,736	3924220,669	203,286	512699,752	3924220,554	204,926
	5	0	1	512747,623	3924166,389	206,227	512747,586	3924166,346	209,043
	6	1	0	512748,647	3923848,65	211,528	512748,645	3923848,65	211,528
	7	0	1	512506,672	3923891,421	218,46	512506,666	3923891,124	217,576
	8	1	0	512390,339	3924087,504	219,545	512390,34	3924087,501	219,545
	9	1	0	512654,232	3924270,943	208,973	512654,233	3924270,946	208,973

Table 1. Accuracy assessment results.

Combination	n	RMSE <sub>x</sub> (m)	RMSE <sub>y</sub> (m)	RMSE <sub>r</sub> (m)	RMSE <sub>z</sub> (m)	Accuracy <sub>r</sub> (m)	Accuracy <sub>z</sub> [NVA] (m)
1	9	0,278	0,216	0,352	0,156	0,627	0,307
2	3	0,186	0,242	0,305	0,297	0,543	0,582
3	4	0,199	0,107	0,226	0,659	0,403	1,291
4	4	0,384	0,406	0,559	1,129	0,995	2,214
5	4	0,188	0,253	0,310	0,286	0,561	0,561
6	5	0,567	0,827	1,002	0,780	1,785	1,528
7	5	0,189	0,223	0,293	1,538	0,521	3,014
8	6	0,185	0,290	0,344	1,438	0,612	2,818

4. Discussion

This study has demonstrated the effectiveness and efficiency of acquiring a large territorial area of 250 hectares in just three working days. This result was achieved using a low-cost UAS, a GNSS antenna, and two operators. The collected data was processed using an automated process as much as possible, achieving excellent results for the needs of a university workshop. The outputs generated, including point clouds, two and three-dimensional DTM and DSM models, orthophotos, and contour lines, provided students with useful tools to refine their analysis of the archaeological-environmental site and to design intervention proposals with different levels of detail. Thanks to the manipulation of this data through various software, the students were able to generate additional 2D and 3D outputs for project purposes.

In this paper, we paid particular attention to the evaluation of the quality and accuracy of the collected data, with the goal of providing a critical assessment that can help identify room for improvement in the workflow for similar jobs that may arise in the future, such as those for the DIACHRONIC LANDSCAPES workshop series.

The analysis of the survey workflow highlighted the enormous potential of UAV flight planning but also emphasized some factors not to underestimate, such as the impact of weather conditions on the estimate of the time and batteries needed for aerial surveying.

The analysis of the photogrammetric data processing workflow demonstrated that Metashape software, despite not being specifically designed for the topographical field (unlike its competitors Zephyr or PIX4D), proved extremely useful in generating the DTM model, both in terms of quality and processing time, the latter aspect being essential considering the time constraints imposed by the workshop.

Finally, the accuracy analysis carried out post-workshop provided important insights into the reliability of the created DTM models, contributing to shed light on important aspects for future work, particularly regarding the combination of photogrammetric and GNSS surveying. Although



we were aware from the start that a survey without a UAV with integrated RTK data would require significant GNSS ground surveying, the time constraints, the available operators, the morphological difficulties, and the limitations posed by the presence of private properties in the area only made possible an essential GNSS survey localized in the main project area, without being able to cover the entire area of the plateau. For this reason, the analysis focused on the area of about 500x500m, whose points were deficient, but still useful for analysis and reflections on future case studies of similar size. It is also important to underline that the GNSS points were detected without the use of specific targets, but by acquiring the coordinates of notable morphological points, which led to less reliability in terms of internal accuracy between points identified in the digital and points detected in the real world.

Moving now to the analysis of the tabular data produced in chapter 3.2, we try to determine what would have been the optimal strategy for the positioning of the GCP and QCP markers. Considering a GSD (Ground Sampling Distance) of 3 cm/pix, obtained from the export quality defined for the orthomosaic, we evaluate the accuracy based on the horizontal and vertical RMSE (Root Mean Square Error), as indicated in various studies in the field.

The “Combination 1” differs from the others in the analysis method adopted, in fact, considering the three methods described in chapter 3.2, this combination is the only one among the 8 to use method 1, which foresees the use of all the GNSS points detected both as GCP and as QCP for the accuracy verification. As already mentioned, it is important to note that this method does not use independent measurements and should therefore be evaluated in terms of internal precision rather than accuracy: in fact, we analyze the residuals from the bundle adjustment once the 3D model has been rotated and scaled, based on the same QCP previously used as GCP. For this reason, we expect a lower RMSE compared to the following combinations, both horizontally and vertically. It is also reasonable to assume that if we considered other QCP points not used as GCP in the bundle adjustment phase, the RMSE values would be higher. The data confirms these preliminary considerations.

In the following combinations, it has been evaluated the accuracy of the 3D model based on method 2, i.e. using a variable number of GCP for the bundle adjustment and the remaining points as QCP, measuring the achieved accuracy in terms of RSME, and evaluating the results of the remaining 7 combinations between GCP and QCP. As also reported in the conclusions of [23], several studies have widely recognized that the greater the number of GCPs, the greater the accuracy measured in the QCPs (e.g., combinations 2-3). Moreover, with equal GCPs, the accuracy increases up to double when the GCPs are optimally positioned (e.g., combinations 3-4-5 and 6-7).

In light of these results, we can draw the following conclusions:

- The number of GNSS points detected and used was useful for the georeferencing of the model, although a high degree of accuracy was not evident in any of the proposed combinations.
- With the UAS technology adopted, a more effective strategy would have involved segmenting the total area into square sub-areas of size between 150x150 and 200x200 meters. Each sub-area would have needed to be structured with 4 GCPs arranged along the perimeter and one centrally positioned GCP. The accuracy analysis carried out on the detail project suggested that for such an area, a total of about 25 GCPs would have been necessary, compared to the 9 actually used. Moreover, we should have arranged at least 3 QCPs per sub-area in a random manner, to ensure adequate accuracy control. Projecting this scheme onto the entire project surface, with approximate dimensions of 1.5x1.5 kilometers, it is estimated that the number of necessary GCPs would have been about 200.
- In the case where, instead of the UAS technology adopted, we had opted for a UAS with integrated RTK, the amount of GNSS points to be detected could have been drastically less. For example, for the complete survey of the plateau, we probably could have limited ourselves to positioning a dozen GCPs along the peripheral areas of the plateau, another group of ten GCPs distributed equidistantly in the central sector, and a dozen QCPs dislocated randomly on the territory. Regarding the detail project, the use of RTK technology would presumably have made the GNSS points identified during the workshop sufficient, despite their not optimal arrangement. In this scenario, we would have used an approach similar to combination n°2.

Considering these factors and evaluating the cost-benefit ratio, probably the best solution would have been to adopt a UAV equipped with integrated RTK technology. This decision would bring a series of significant advantages.

Below we illustrate the main ones, comparing the DJI Mini 3 Pro (the latest version of the UAV used in our workshop) with the DJI Mavic 3E, equipped with RTK technology:

- Using RTK technology, the number of points to be detected on the ground would be less, with a consequent contraction of the times associated with GNSS surveying and a corresponding reduction in the costs related to the workforce used for the operation.
- In cases where points are located in areas not easily accessible, their detection could be avoided without significantly affecting the overall accuracy.
- The high resolution of the camera integrated in the UAV Mavic 3E RTK would bring a series of advantages. For example, keeping the GSD constant, it would have been possible to fly at higher altitudes, thus reducing the number of photos and stripes needed. This would have led to a reduction in acquisition times on site and photogrammetric reconstruction in the office.

However, considering the expected benefits and the extent of the territory subject to our study, the price ratio between the DJI Mini 3 Pro and the DJI Mavic 3E RTK would seem to amply justify the investment in the latter.

In summary, this research has highlighted the vast opportunities offered by low-cost aerial photogrammetry, while also emphasizing the fundamental importance of a precise complementary GNSS surveying work to ensure the accuracy of the results. The results achieved have provided a crucial contribution in achieving the objectives of the workshop. Future projects, concerning the same area, could take advantage of the data already collected during this workshop, although it might be necessary to consider the integration of additional GNSS data to increase the accuracy of the work done so far.

**Author Contributions:** Conceptualization, M.M. and A.S.; methodology, M.M. and A.S.; software, A.S.; validation, M.M. and A.S.; formal analysis, A.S.; investigation, M.M. and A.S.; resources, M.M.; data curation, A.S.; writing—original draft preparation, A.S.; writing—review and editing, M.M.; visualization, A.S.; supervision, M.M.; project administration, M.M.; funding acquisition, M.M. All authors have read and agreed to the published version of the manuscript.

**Funding:** This research was funded by the Department of Architecture of the University of Ferrara under the “Fondo per l’Incentivazione alla Ricerca Dipartimentale” - FIRD 2022.

**Data Availability Statement:** The data presented in this study are available on request from the corresponding author.

**Acknowledgments:** We would like to express our gratitude to Prof. Dimitris Tsakalakis of the CAM (Center for Mediterranean Architecture), Prof. Prof. Panita Karanamea of the TUC (Technological University of Crete School of Architecture), and Prof. Gianni Lobosco and Prof. Elena Dorato of the UNIFE (University of Ferrara Department of Architecture) for contributing in the organization and realization of the DIACHRONIC LANDSCAPES International Design Workshop, as well as all the students participating in it. We would like to thank also the INCEPTION s.r.l., spin-off company of the University of Ferrara, for providing the UAS equipment and Prof. Panagiotis Partsinevelos of the Senselab Space Informatics office of the Technical University of Crete for providing the GNSS equipment.

**Conflicts of Interest:** The authors declare no conflict of interest.

## References

1. Mora, O.E.; Suleiman, A.; Chen, J.; Pluta, D.; Okubo, M.H.; Josenhans, R. Comparing SUAS Photogrammetrically-Derived Point Clouds with GNSS Measurements and Terrestrial Laser Scanning for Topographic Mapping. *Drones* **2019**, *3*, 64, doi:10.3390/drones3030064.
2. Jiménez-Jiménez, S.I.; Ojeda-Bustamante, W.; Marcial-Pablo, M. de J.; Enciso, J. Digital Terrain Models Generated with Low-Cost UAV Photogrammetry: Methodology and Accuracy. *ISPRS International Journal of Geo-Information* **2021**, *10*, 285, doi:10.3390/ijgi10050285.
3. Remondino, F.; Barazzetti, L.; Nex, F.; Scaioni, M.; Sarazzi, D. UAV PHOTOGRAMMETRY FOR MAPPING AND 3D MODELING – CURRENT STATUS AND FUTURE PERSPECTIVES. *The International Archives of the Photogrammetry, Remote Sensing and Spatial Information Sciences* **2012**, XXXVIII-1-C22, 25–31, doi:10.5194/isprsarchives-XXXVIII-1-C22-25-2011.

4. Westoby, M.J.; Brasington, J.; Glasser, N.F.; Hambrey, M.J.; Reynolds, J.M. 'Structure-from-Motion' Photogrammetry: A Low-Cost, Effective Tool for Geoscience Applications. *Geomorphology* **2012**, *179*, 300–314, doi:10.1016/j.geomorph.2012.08.021.
5. Guth, P.L.; Van Niekerk, A.; Grohmann, C.H.; Muller, J.-P.; Hawker, L.; Florinsky, I.V.; Gesch, D.; Reuter, H.I.; Herrera-Cruz, V.; Riazanoff, S.; et al. Digital Elevation Models: Terminology and Definitions. *Remote Sensing* **2021**, *13*, 3581, doi:10.3390/rs13183581.
6. Pratibha P. Shingare; Sumit S. Kale; Review on Digital Elevation Model. *International Journal of Modern Engineering Research (IJMER)* **2013**, *3*, 2412-2418
7. Digital Terrain Mapping and Analysis - Ppt Download Available online: <https://slideplayer.com/slide/5153395/> (accessed on 8 June 2023).
8. Polat, N.; Uysal, M. DTM GENERATION WITH UAV BASED PHOTOGRAMMETRIC POINT CLOUD. *The International Archives of the Photogrammetry, Remote Sensing and Spatial Information Sciences* **2017**, *XLII-4-W6*, 77–79, doi:10.5194/isprs-archives-XLII-4-W6-77-2017.
9. Abdullah, A.F.; Vojinovic, Z.; Price, R.K.; Aziz, N.A.A. Improved Methodology for Processing Raw LiDAR Data to Support Urban Flood Modelling – Accounting for Elevated Roads and Bridges. *Journal of Hydroinformatics* **2011**, *14*, 253–269, doi:10.2166/hydro.2011.009.
10. Barazzetti, L.; Brovelli, M.A.; Valentini, L. LiDAR Digital Building Models for True Orthophoto Generation. *Appl Geomat* **2010**, *2*, 187–196, doi:10.1007/s12518-010-0034-9.
11. Trepekli, K.; Balstrøm, T.; Friborg, T.; Fog, B.; Allotey, A.N.; Kofie, R.Y.; Møller-Jensen, L. UAV-Borne, LiDAR-Based Elevation Modelling: A Method for Improving Local-Scale Urban Flood Risk Assessment. *Nat Hazards* **2022**, *113*, 423–451, doi:10.1007/s11069-022-05308-9.
12. Mazzoleni, M.; Paron, P.; Reali, A.; Juizo, D.; Manane, J.; Brandimarte, L. Testing UAV-Derived Topography for Hydraulic Modelling in a Tropical Environment. *Nat Hazards* **2020**, *103*, 139–163, doi:10.1007/s11069-020-03963-4.
13. Gil-Docampo, M.L.; Arza-García, M.; Ortiz-Sanz, J.; Martínez-Rodríguez, S.; Marcos-Robles, J.L.; Sánchez-Sastre, L.F. Above-Ground Biomass Estimation of Arable Crops Using UAV-Based SfM Photogrammetry. *Geocarto International* **2020**, *35*, 687–699, doi:10.1080/10106049.2018.1552322.
14. Dzierżek, J.; Kaczorowski, J.; Szymanek, M. Advantages of High-Resolution Digital Terrain Model (DTM) Analysis in Geological Cartography 2016.
15. Hugenholtz, C.H.; Whitehead, K.; Brown, O.W.; Barchyn, T.E.; Moorman, B.J.; LeClair, A.; Riddell, K.; Hamilton, T. Geomorphological Mapping with a Small Unmanned Aircraft System (SUAS): Feature Detection and Accuracy Assessment of a Photogrammetrically-Derived Digital Terrain Model. *Geomorphology* **2013**, *194*, 16–24, doi:10.1016/j.geomorph.2013.03.023.
16. Dubbini, M.; Curzio, L.L.; Campedelli, A. Digital Elevation Models from Unmanned Aerial Vehicle Surveys for Archaeological Interpretation of Terrain Anomalies: Case Study of the Roman Castrum of Burnum (Croatia). *Journal of Archaeological Science: Reports* **2016**, *8*, 121–134, doi:10.1016/j.jasrep.2016.05.054.
17. Rusnák, M.; Sládek, J.; Buša, J.; Greif, V. Suitability of Digital Elevation Models Generated by Uav Photogrammetry for Slope Stability Assessment (Case Study of Landslide in Svätý Anton, Slovakia). *Acta Scientiarum Polonorum Formatio Circumiectus* **2016**, *15*, 439–450, doi:10.15576/ASP.FC/2016.15.4.439.
18. Ariza López, F.J.; Atkinson Gordo, A.D. Analysis of Some Positional Accuracy Assessment Methodologies. *Journal of Surveying Engineering* **2008**, *134*, 45–54, doi:10.1061/(ASCE)0733-9453(2008)134:2(45).
19. Sanz-Ablanedo, E.; Chandler, J.H.; Rodríguez-Pérez, J.R.; Ordóñez, C. Accuracy of Unmanned Aerial Vehicle (UAV) and SfM Photogrammetry Survey as a Function of the Number and Location of Ground Control Points Used. *Remote Sensing* **2018**, *10*, 1606, doi:10.3390/rs10101606.
20. Tzanakaki, K. Απτερά Το Ταφικό Μνημείο II: Ανασκαφικά Δεδομένα Και Ερμηνευτική Προσέγγιση. *Η Ελεύθερα, η Κρήτη και ο Εξω Κόσμος/ Eleutherna, Crete and the Outside World. Πρακτικά Διεθνούς Αρχαιολογικού Συνεδρίου (Πέθυμνο 2018) Ν. Χρ. Σταμπολίδης, Μ. Γιαννοπούλου (επιμ.)* **2020**.

**Disclaimer/Publisher's Note:** The statements, opinions and data contained in all publications are solely those of the individual author(s) and contributor(s) and not of MDPI and/or the editor(s). MDPI and/or the editor(s) disclaim responsibility for any injury to people or property resulting from any ideas, methods, instructions or products referred to in the content.